applied sciences

MDPI

Article

Light Harvesting in Silicon Nanowires Solar Cells by Using Graphene Layer and Plasmonic Nanoparticles

Ali Elrashidi [1,2]

[1] Department of Electrical Engineering, University of Business and Technology, Jeddah 21432, Saudi Arabia; a.elrashidi@ubt.edu.sa
[2] Department of Engineering Physics, Alexandria University, Alexandria 21544, Egypt

Abstract: In this work, a silicon nanowire solar cell for efficient light harvesting in the visible and near-infrared regions is introduced. In this structure, the silicon nanowires (SiNWs) are coated with a graphene layer and plasmonic nanoparticles are distributed on the top surface of the silicon substrate layer. The proposed structure is simulated using the finite difference time domain (FDTD) method to determine the performance of the solar cell by calculating the open-circuit voltage, fill factor, short-circuit current density, and power conversion efficiency. The absorbed light energy is compared for different nanoparticle materials, namely Au, Ag, Al, and Cu, and Au NPs give the best performance. Different values of the radius of the Au NP are simulated, namely 30, 40, 50, and 60 nm, to determine the optimum radius, and the effect of excess carrier concentration on the solar cell performance is also tested. The obtained open-circuit voltage is 0.63 V, fill factor is 0.73, short-circuit current density is 41.7 mA/cm^2, and power conversion efficiency is 19.0%. The proposed SiNW solar cell improves the overall efficiency by almost 60%. Furthermore, the effects of the NW length and distance between NWs are also studied in this work. Finally, the distribution of the optical power in different layers along the solar cell and for different solar cell structures is also illustrated in this paper.

Keywords: plasmonic nanoparticles; silicon solar cell; graphene; short-circuit current density; open-circuit voltage; power conversion efficiency

Citation: Elrashidi, A. Light Harvesting in Silicon Nanowires Solar Cells by Using Graphene Layer and Plasmonic Nanoparticles. *Appl. Sci.* **2022**, *12*, 2519. https://doi.org/10.3390/app12052519

Academic Editors: Angela Malara, Patrizia Frontera and Antonio Di Bartolomeo

Received: 7 February 2022
Accepted: 27 February 2022
Published: 28 February 2022

1. Introduction

Crystalline silicon nanowires (SiNWs) usually exhibit a highly efficient light absorption and an antireflection of the incident light greater than that of a flat surface silicon material of the same size [1]. Geometrical scattering and antenna effect of the SiNWs are the main reasons for high light-harvesting performance [2,3], where the NW density and diameter determine the absorbed wavelength, which is called the resonance wavelength [4]. One more advantage of the SiNW solar cell is the simplicity of the fabrication process with a large-area scalable structure, as introduced by Garnett and Yang [5]. This process produced a high open-circuit voltage value, V_{oc}, and high fill factor, FF, which lead to producing higher overall efficiency, μ, of the solar cell for high values of short-circuit current density, J_{sc}. However, we still need to increase the value of the J_{sc}, which can be obtained by using an absorber layer, such as graphene, C [6]. For its good electric properties, as a thin and highly transparent material, graphene has been greatly used in recent research [7]. Graphene on a silicon surface forms a Schottky junction solar cell with a very low efficiency, which can be improved by engineering the interface with a passivation layer to increase the graphene work function [8]. On the other hand, plasmonic nanoparticles have high absorption properties which depend on the surrounding medium and the size, shape, and material of the nanoparticles [9]. In this work, we used a graphene layer and plasmonic NPs distributed on the top of a silicon surface to enhance the power conversion efficiency (PCE) of the SiNW solar cell [10–12].

Large-area SiNWs with radial PN junctions have been produced using a simple fabrication method by Garnett and Yang [5]. The fabricated solar cell was based on a room-temperature aqueous etching method and low-temperature thin film deposition with a rapid thermal annealing crystallization process. The given method increased the PCE to be 5.3% with V_{oc} = 0.56 V, FF = 0.607, and J_{sc} = 17.32 mA/cm^2.

A SiNW solar cell grown on a silicon base and covered with an on-site graphene layer for Schottky junction was introduced by Wallace et al. [6]. The graphene layer increased the carrier collection and enhanced the solar cell efficiency to be 3.83%. The obtained open-circuit voltage is 0.47 V, the fill factor is 0.59, and the short-circuit current density is 13.7 mA/cm^2. Linwei Yu and Pere Cabarrocas fabricated a SiNW nanostructure on a silicon base photovoltaic, which achieved light absorption [1]. In addition, a 3D radial junction solar cell has been developed in order to overcome light-induced degradation. The experimental results illustrated that the maximum obtained open-circuit voltage from the solar cell is 0.82 V and the FF is 0.73, while the short-circuit current density is 15.2 mA/cm^2, which leads to a power conversion efficiency of 9.3%. A large-scale silicon solar microcell fabricated from bulk wafers using transferring printing technique was presented by Yoon et al. [13]. The produced device has many features such as mechanical flexibility, transparency, and ultrathin microconcentrator designs. Theoretical and experimental electrical, mechanical, and optical characteristics of several types of modules were illustrated in this work. The measured V_{oc} is 0.51, FF is 0.61, J_{sc} is 33.6 mA/cm^2, and PCE is 11.6%.

Augusto et al. showed the analytical model of the recombination mechanisms of a silicon solar cell with low bandgap-voltage offset [14]. The work showed the effect of changing excess carrier density on the effective lifetime of the carriers. The untextured structure, with 50 µm thickness, produced 0.764 V as an open-circuit voltage, a fill factor of 0.86, and a short-circuit current density of 38.8 mA/cm^2.

Moreover, the surface plasmon localization (SPL) technique on plasmonic nanoparticles is used as an efficient method to improve the optical absorption of solar cells, metal–dielectric–metal, and metamaterial applications [15–19]. The NP shapes and materials are the main parameters that affect the solar cell and sensor performance [20–23].

In this paper, the light harvesting of SiNW solar cells has been improved by using a graphene layer and gold nanoparticles. Short-circuit current density, power conversion efficiency, and light absorption are simulated by applying a finite difference time domain method using the Lumerical FDTD solutions software package. The effect of changing excess carrier concentration on the PCE is also illustrated in this work. For different nanoparticle materials, the light absorption and PCE are illustrated as a function of the wavelengths. Moreover, the effects of NW length and separation between two successive NWs are also given in this work. In addition, the optical power distribution in different monitoring layers for different proposed solar cell structures is given in this work.

2. Analytical Model

The overall solar cell efficiency can be calculated using a single diode model and by applying the Green empirical expression [4]. Short-circuit current density, J_{sc}, can be calculated using Equation (1) by assuming that an incident photon will produce an electron [9].

$$J_{sc} = \frac{q}{hc} \int I(\lambda) A(\lambda) \lambda \, d\lambda \quad (1)$$

where q is the electron charge, h is the Planck constant, c is the speed of light, $I(\lambda)$ is the standard air mass 1.5 (AM1.5) spectral irradiance, and $A(\lambda)$ is the optical absorption. On the other hand, the open-circuit voltage, V_{oc}, of silicon nanowire pillars is given by Equation (2) [24].

$$V_{OC} = V_{Th} \ln[\frac{\Delta n(N_A + \Delta n)}{n_i^2}] \quad (2)$$

where V_{Th} is the thermal voltage which equals 25.8 mV, N_A is the doping concentration (N_A = 3.3 × 10^{17} cm^{-3}), Δn is the excess carrier concentration for n-type ($\Delta n = 10^{15}$ cm^{-3}) [11],

and n_i is the intrinsic carrier concentration. The open-circuit voltage of the silicon nanowires can be calculated and considered as a fixed value equal to 0.626 V as it depends on the energy level of the material and for $n_i = 10^{10}$ cm^{-3} at room temperature.

Hence, the fill factor can be calculated using Equation (3) [9].

$$FF = \frac{\frac{V_{oc}}{V_{Th}} - \ln\left(\frac{V_{oc}}{V_{Th}} + 0.72\right)}{\frac{V_{oc}}{V_{Th}} + 1} \quad (3)$$

The maximum output power, P_{max}, can be calculated using Equation (4).

$$P_{max} = J_{sc} \times V_{oc} \times FF \quad (4)$$

Hence, the overall solar cell efficiency, η, can be calculated as a ratio of maximum output power to solar input power.

Gold, Au, plasmonic nanoparticles distributed on the substrate layer will change the optical power absorbed in the active layer and depend on the maximum value of reflectivity. Nanoparticle shape has a great effect on the transmitted optical power as well as the relative permittivity of the gold nanoparticles and the dielectric function of the surrounding medium [9]. The maximum reflectivity can be calculated using Equation (5).

$$\lambda_{max} = \frac{L}{g}\left(\frac{\varepsilon_{Au}\varepsilon_m(\lambda_{max})}{\varepsilon_m + \varepsilon_{Au}(\lambda_{max})}\right)^{1/2} \quad (5)$$

where ε_m is the permittivity of the surrounding medium, ε_{Au} is a gold nanoparticle dielectric constant at corresponding λ_{max}, g is an integer, and L is structural periodicity. Hence, the dielectric permittivity can be expressed by using a multioscillator Drude–Lorentz model [9] as given in Equation (6):

$$\varepsilon_{Au} = \varepsilon_\infty - \frac{\omega_D^2}{\omega^2 + j\omega\gamma_D} - \sum_{k=1}^{6} \frac{\delta_k \omega_k^2}{\omega^2 - \omega_k^2 + 2j\omega\gamma_k} \quad (6)$$

where ε_∞ is the gold high-frequency dielectric permittivity, ω_D and γ_D are the plasma and collision frequencies of the free electron gas, δ_k is the amplitude of Lorentz oscillator, ω_k is the resonance angular frequencies, and γ_k is the damping constants for k value from 1 to 6.

3. Proposed Structure

In this work, we used an electromagnetic wave solver, Lumerical FDTD solutions software, to design and analyze the proposed structure. A unit cell of the proposed structure has been simulated using the FDTD method. The overall dimensions of the unit cell are $500 \times 500 \times 700$ nm^3 in the three dimensions x, y, and z, respectively. A silicon substrate with height h_2 = 3 µm is placed on the top of a back oxide material with height h_1 = 1 µm, as illustrated in Figure 1. Silicon nanowires are grown on the top of the silicon substrate with height H = 5 µm and period P = 550 nm between each NW. In addition to that, a graphene layer can be used on the top of substrate material and on the NWs as well.

The boundary conditions are considered as periodic structures in x-direction and y-direction, as the structure is extended in both x- and y-dimensions, and perfect matching layer in z-direction, as the structure is not repeated in z-direction, where the minimum mesh size is 20 nm in all directions. A plane wave source with wavelength band 400–1100 nm and offset time 7.5 fs is used as a light source. In addition, the solar generation calculation region is given in the active layer to calculate the short-circuit current density.

The refractive index of back oxide is 1.4; however, the value for silicon is a function of the wavelength and follows the Aspnes and Studna model [25], and the refractive index of graphene follows the Phillip and Taft model [26]. On the other hand, the refractive index of plasmonic NPs is summarized using Equation (6) in Table 1 [27].

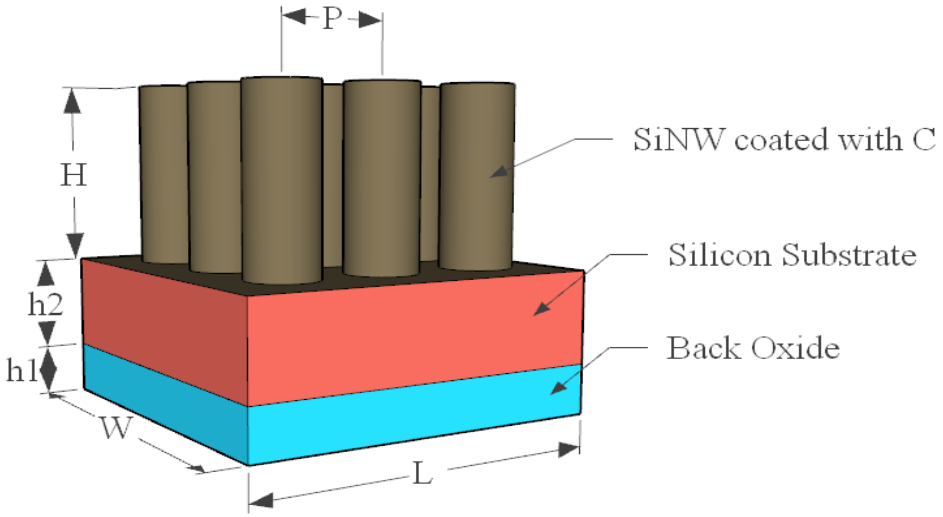

Figure 1. Schematic diagram of the proposed structure.

Table 1. Plasmonic parameters used for the metallic nanoparticle.

Material	Term	Strength	Plasma Frequency	Resonant Frequency	Damping Frequency
Ag	0	0.8450	$0.136884 \times 10^{+17}$	$0.000000 \times 10^{+00}$	$0.729239 \times 10^{+14}$
	1	0.0650	$0.136884 \times 10^{+17}$	$0.123971 \times 10^{+16}$	$0.590380 \times 10^{+16}$
	2	0.1240	$0.136884 \times 10^{+17}$	$0.680775 \times 10^{+16}$	$0.686701 \times 10^{+15}$
	3	0.0110	$0.136884 \times 10^{+17}$	$0.124351 \times 10^{+17}$	$0.987512 \times 10^{+14}$
	4	0.8400	$0.136884 \times 10^{+17}$	$0.137993 \times 10^{+17}$	$0.139163 \times 10^{+16}$
	5	5.6460	$0.136884 \times 10^{+17}$	$0.308256 \times 10^{+17}$	$0.367506 \times 10^{+16}$
Au	0	0.7600	$0.137188 \times 10^{+17}$	$0.000000 \times 10^{+00}$	$0.805202 \times 10^{+14}$
	1	0.0240	$0.137188 \times 10^{+17}$	$0.630488 \times 10^{+15}$	$0.366139 \times 10^{+15}$
	2	0.0100	$0.137188 \times 10^{+17}$	$0.126098 \times 10^{+16}$	$0.524141 \times 10^{+15}$
	3	0.0710	$0.137188 \times 10^{+17}$	$0.451065 \times 10^{+16}$	$0.132175 \times 10^{+16}$
	4	0.6010	$0.137188 \times 10^{+17}$	$0.653885 \times 10^{+16}$	$0.378901 \times 10^{+16}$
	5	4.3840	$0.137188 \times 10^{+17}$	$0.202364 \times 10^{+17}$	$0.336362 \times 10^{+16}$
Cu	0	0.5750	$0.164535 \times 10^{+17}$	$0.000000 \times 10^{+00}$	$0.455775 \times 10^{+14}$
	1	0.0610	$0.164535 \times 10^{+17}$	$0.442101 \times 10^{+15}$	$0.574276 \times 10^{+15}$
	2	0.1040	$0.164535 \times 10^{+17}$	$0.449242 \times 10^{+16}$	$0.160433 \times 10^{+16}$
	3	0.7230	$0.164535 \times 10^{+17}$	$0.805202 \times 10^{+16}$	$0.488135 \times 10^{+16}$
	4	0.6380	$0.164535 \times 10^{+17}$	$0.169852 \times 10^{+17}$	$0.654037 \times 10^{+16}$
Al	0	0.5230	$0.227583 \times 10^{+17}$	$0.000000 \times 10^{+00}$	$0.714047 \times 10^{+14}$
	1	0.2270	$0.227583 \times 10^{+17}$	$0.246118 \times 10^{+15}$	$0.505910 \times 10^{+15}$
	2	0.0500	$0.227583 \times 10^{+17}$	$0.234572 \times 10^{+16}$	$0.474006 \times 10^{+15}$
	3	0.1660	$0.227583 \times 10^{+17}$	$0.274680 \times 10^{+16}$	$0.205251 \times 10^{+16}$
	4	0.0300	$0.227583 \times 10^{+17}$	$0.527635 \times 10^{+16}$	$0.513810 \times 10^{+16}$

4. Results and Discussion

To maximize the absorbed light in the visible and NIR regions, which leads to an increase in the J_{sc} and the overall frequency, different proposals will be produced. The absorption of a traditional SiNW solar cell will be compared to SiNWs coated with a 2D graphene layer and with/without Au plasmonic nanoparticles distributed on the silicon substrate layer. Figure 2a,b illustrates the absorption and transmission of the four proposed techniques. As shown in Figure 2a, the absorptions of the traditional SiNWs and of SiNWs coated with graphene are almost the same; however, a high absorption has been obtained when Au NPs are distributed on the top silicon substrate surface. The light transmitted through the solar cell is illustrated given in Figure 2b. However, it is very hard to distinguish

between four cases, so the short-circuit current density and consequently PCE is the used in such case to choose which structure has better performance.

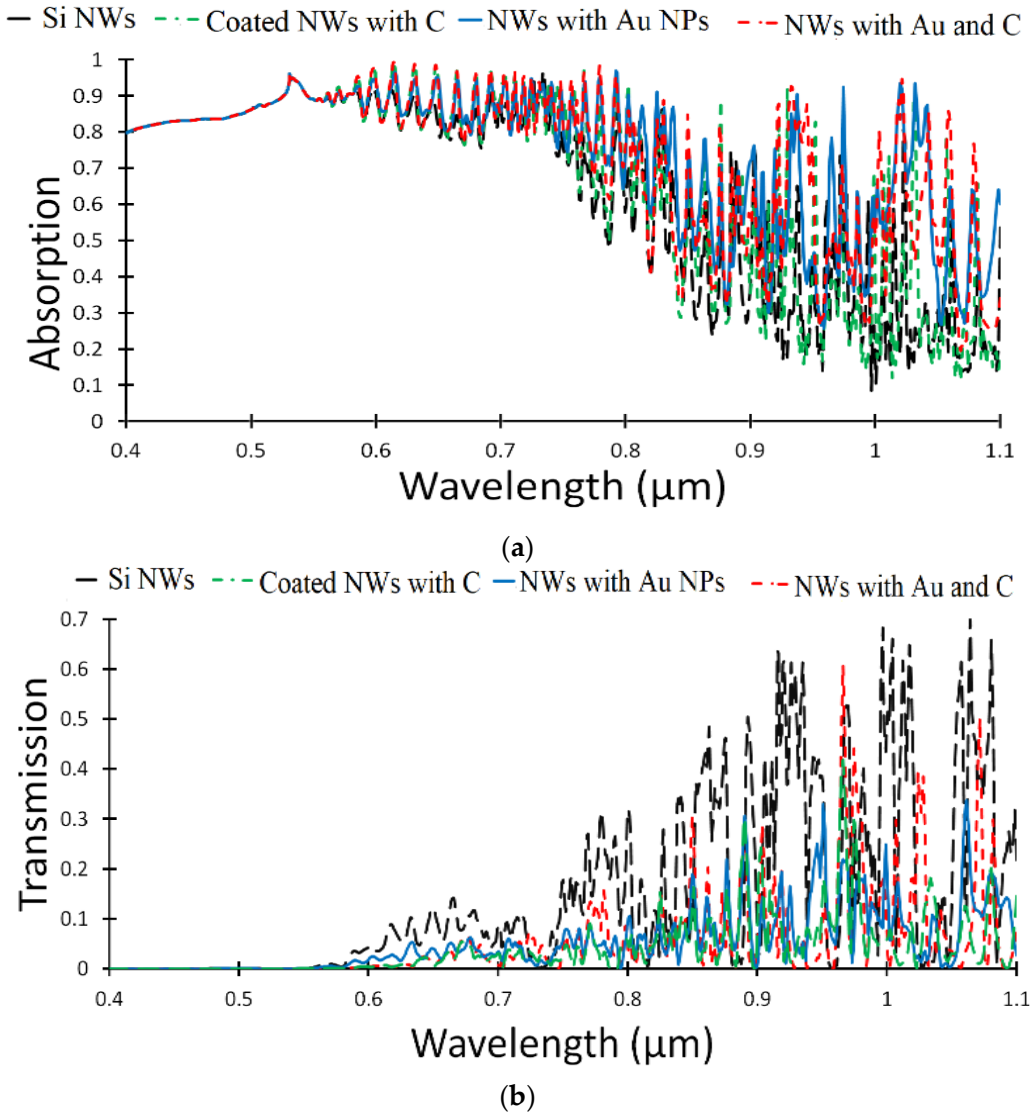

Figure 2. (**a**) Absorption and (**b**) transmission of the four proposed structures: traditional SiNWs, SiNWs coated with a graphene layer, SiNWs with Au NPs distributed on the substrate, and SiNWs with graphene layer and Au NPs.

The resultant short-circuit current density and the power conversion efficiency for each structure are given in Table 2. The maximum J_{sc}, 34.72 mA/cm^2, is obtained when the SiNWs coated with a graphene layer and Au NPs are distributed on the silicon substrate surface, which gives maximum overall efficiency, 15.8%, as shown in Table 2.

Table 2. Short-circuit current density and overall efficiency of the proposed four structures.

Proposed Structure	J_{sc} (mA/cm^2)	PCE (%)
Traditional SiNWs	31.56	14.40
SiNWs coated with graphene layer	31.91	14.60
SiNWs with Au NPs	33.20	15.10
SiNWs with graphene layer and Au NPs	34.72	15.80

The absorbed light is increased and the short-circuit current density and power conversion efficiency are consequently increased as the graphene layer is added, due to its

high absorption properties. On the other hand, adding Au NPs increased the absorbed light according to Equations (5) and (6). To compare between the given two structures, SiNWs with Au NPs and with/without graphene layer, the absorption and transmission are illustrated in Figure 3a,b.

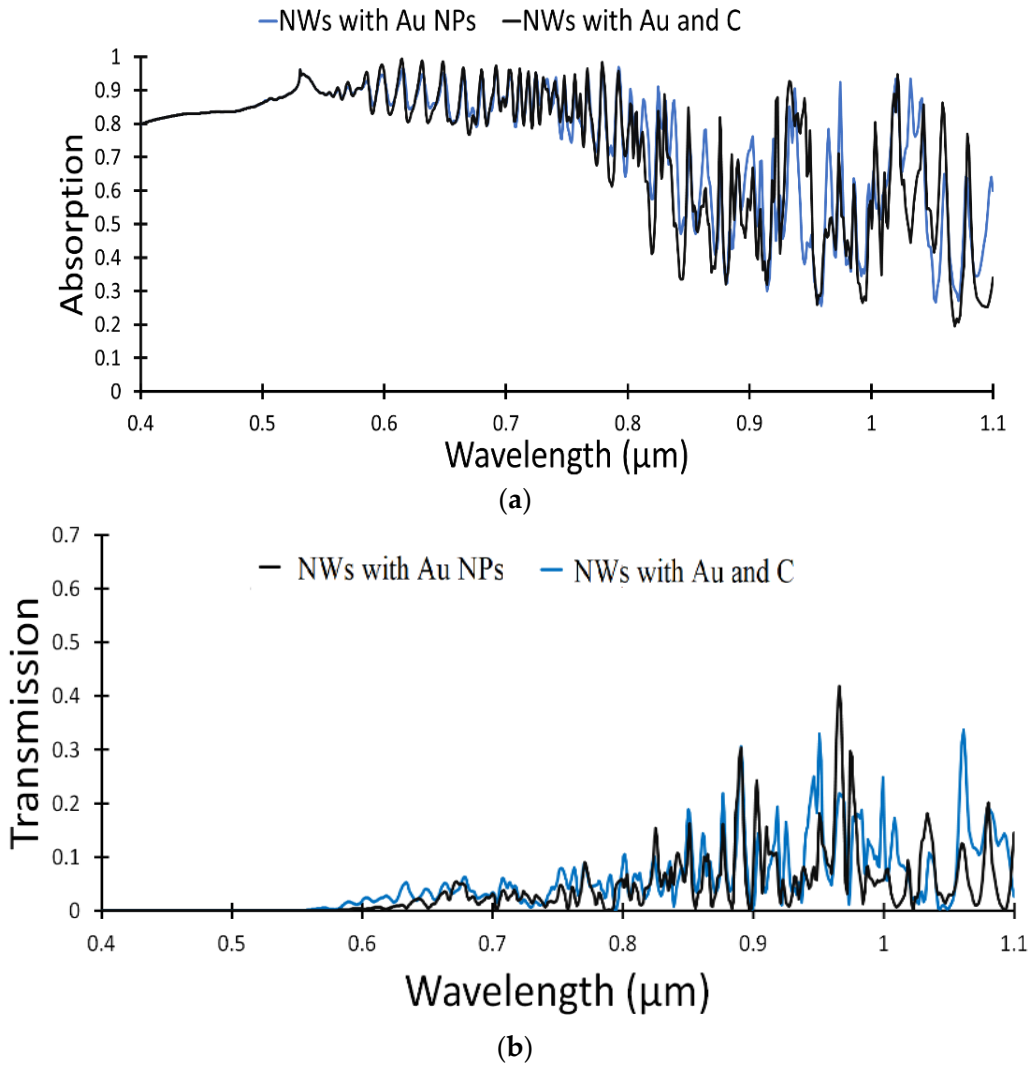

Figure 3. (**a**) Absorption and (**b**) transmission of the main two structures: SiNWs with Au NPs distributed on the substrate and SiNWs with graphene layer and Au NPs.

To increase the efficiency of the solar cell, Au NPs are distributed on the top silicon surface directly, without using the graphene layer, and the graphene layer is used to coat the top surface of the SiNWs, as illustrated in Figure 4a,b. The obtained short-circuit current density is 41.7 mA/cm^2 and the overall solar cell efficiency is 19.0%. A 3D structure of the configuration using the graphene layer is shown in Figure 4a, and the side view of the structure is given in Figure 4b. The graphene layer, on the top of NWs, absorbs the incident light and retransmits it into the NWs, which behave as nanoantennas, while the plasmonic Au NPs absorb the light and transfer it to the silicon substrate.

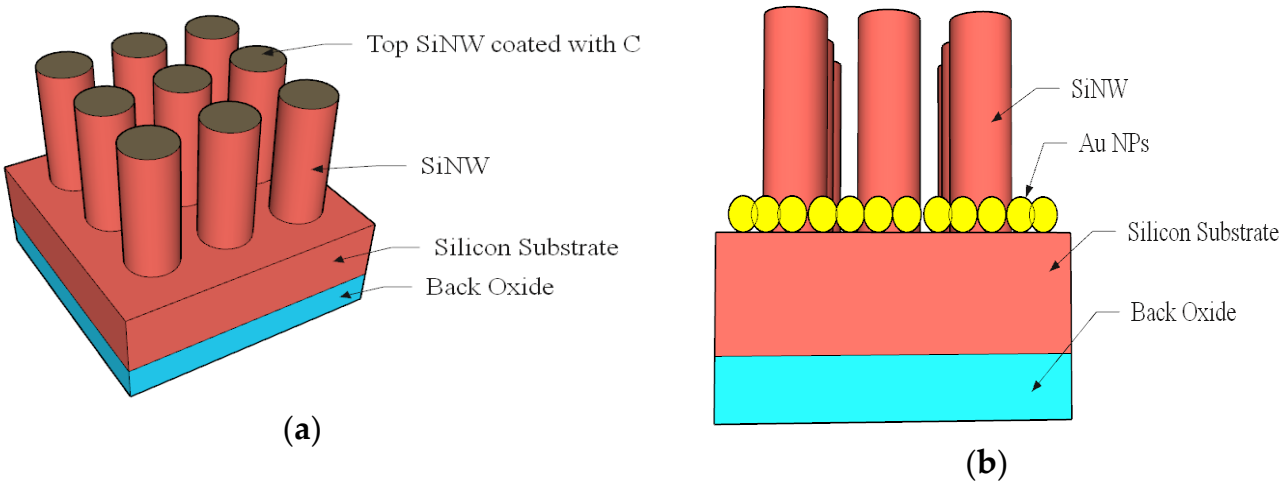

Figure 4. (**a**) Graphene layer coats the top SiNWs surface; (**b**) Au NPs distributed on the top of the silicon substrate.

Figure 5 shows the absorption, reflectance, and transmission of the incident light on the proposed SiNW solar cell illustrated in Figure 4.

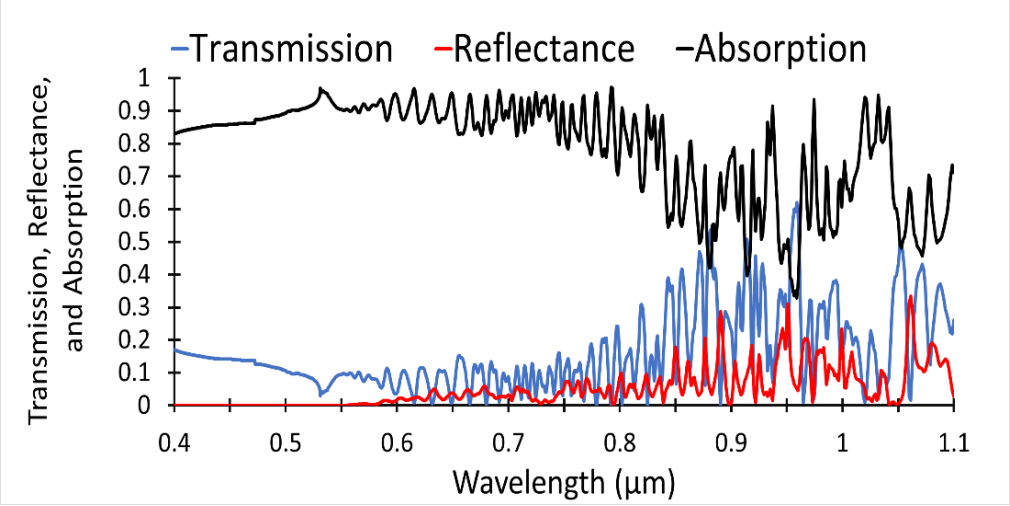

Figure 5. Percentage of absorption, reflectance, and transmission of the SiNWs with a graphene layer on the top of NWs and Au NPs distributed on the silicon substrate.

The reflected and transmitted optical power have been obtained from the simulation analysis by using frequency-domain field and power monitors. Then, the absorption could be calculated using the formula ($A = 1 - T - R$), where T, R, and A are the transmitted, reflected, and absorbed optical power. The absorption is enhanced in the NIR region, which leads to increases in the short-circuit current and power conversion efficiency.

The excess carrier concentration (ECC) has a great effect on the solar cell performance as it determines the open-circuit voltage, *FF*, and solar cell efficiency. Figure 6 shows the effect of excess carrier concentration on the PCE of the solar cell, which increased with the increase in the excess carrier concentration.

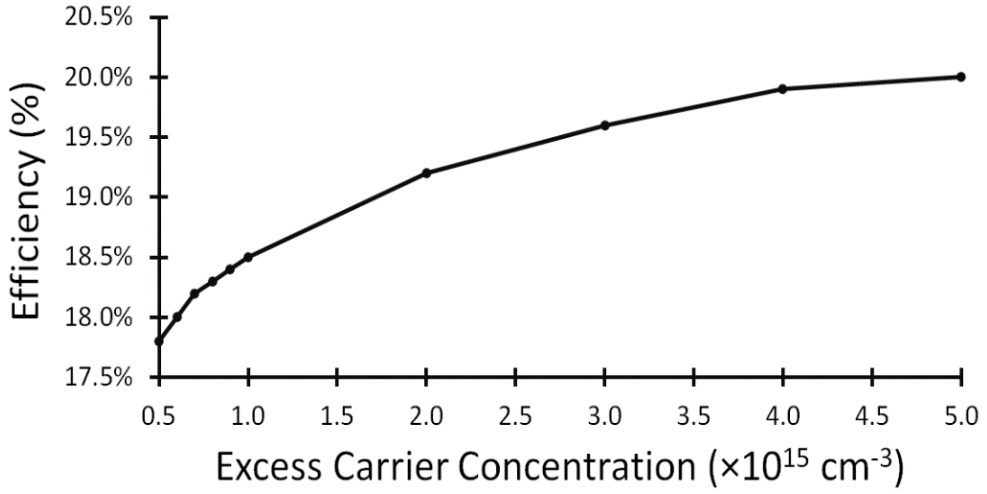

Figure 6. Excess carrier concentration as a function of the PCE for the proposed solar cell structure.

The open-circuit voltage, *FF*, and PCE are illustrated in Table 3 for different excess carrier concentrations.

Table 3. Open-circuit voltage, *FF*, and overall efficiency for the proposed structure.

Excess Carrier Concentration ($\times 10^{-15}$ cm^{-3})	V_{oc} (V)	FF	PCE (%)
0.5	0.61	0.72	17.8
0.6	0.61	0.73	18.0
0.7	0.62	0.73	18.2
0.8	0.62	0.73	18.3
0.9	0.62	0.73	18.4
1.0	0.63	0.73	19.0
2.0	0.64	0.73	19.2
3.0	0.66	0.74	19.6
4.0	0.66	0.74	19.9
5.0	0.67	0.74	20.0

As illustrated in Table 3, the efficiency is increased with the increase in the excess carrier concentration and reaches 20% for ECC equal to 5.0×10^{-15} cm^{-3}. However, the ECC value is strongly related to the effective lifetime of the carriers, where the maximum value of the effective lifetime is 3 ms, which is obtained at ECC = 1×10^{-15} cm^{-3}.

The NP material plays a very important role, as illustrated in Equation (6), which consequently changes the J_{sc} and μ values. Figure 7 shows the absorbed energy for different NP materials, namely Au, Ag, Al, and Cu. In the visible region, the absorptions of all NP materials are almost the same, very close to each other, and one cannot distinguish between them, so the main factor in determining the best material is the short-circuit current density and consequently the PCE.

Gold NPs produce a high J_{sc} and PCE, while silver and copper have J_{sc} values equal to 37.6 and 37.4 mA/cm^2, respectively, as clearly given in Table 4. Aluminum NPs give a short-circuit current density of 33.1 mA/cm^2 and overall efficiency of 15.1%. The maximum obtained power conversion efficiency is 19.0% at short-circuit current density J_{sc} = 41.7 mA/cm^2.

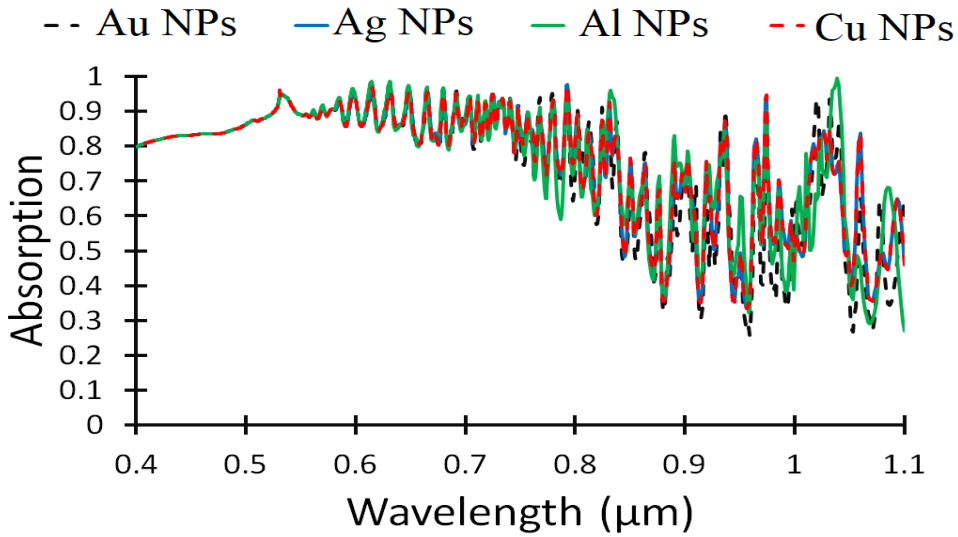

Figure 7. Absorbed energy as a function of wavelength for different NP materials.

Table 4. Short-circuit current density and overall efficiency for different NP materials.

NPs Material	J_{sc} (mA/cm^2)	PCE (%)
Gold, Au	41.7	19.0
Silver, Ag	37.6	17.1
Aluminum, Al	33.1	15.1
Cupper, Cu	37.4	17.0

Plasmonic nanoparticle radius is also considered as one of the main factors that affect solar cell performance. Figure 8 shows the absorbed energy for different Au NP radii, namely 30, 40, 50, and 60 nm. Due to the oscillation of the absorbed power in the NIR region, no distinction between different radii can be considered, so the short-circuit current density is the main factor of choice. The maximum performance, J_{sc} of 41.6 mA/cm^2 and μ of 19.0%, has been obtained at 50 nm Au NP radius, as introduced in Table 5.

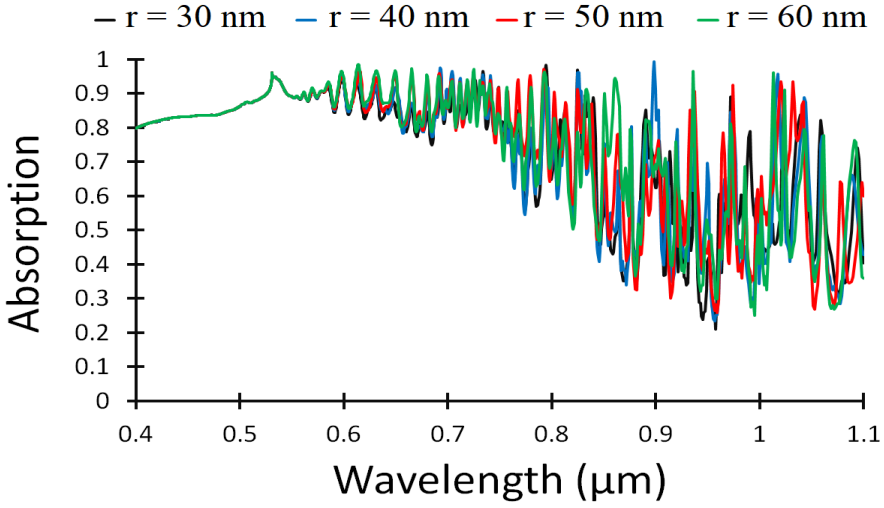

Figure 8. Light absorption (%) as a function of wavelength for different NP radii.

Table 5. Au NP density, short-circuit current density, and overall efficiency for different NP materials.

R (nm)	Au NP Density	J_{sc} (mA/cm^2)	PCE (%)
30	26.0%	34.0	15.5
40	46.0%	34.6	14.4
50	73.0%	41.7	19.0
60	88.4%	33.2	15.1

Figure 9 gives the density of the distributed Au NPs (%) for different radii; the maximum performance of the solar cell is obtained at an NP radius equal to 50 nm, as shown in Table 5.

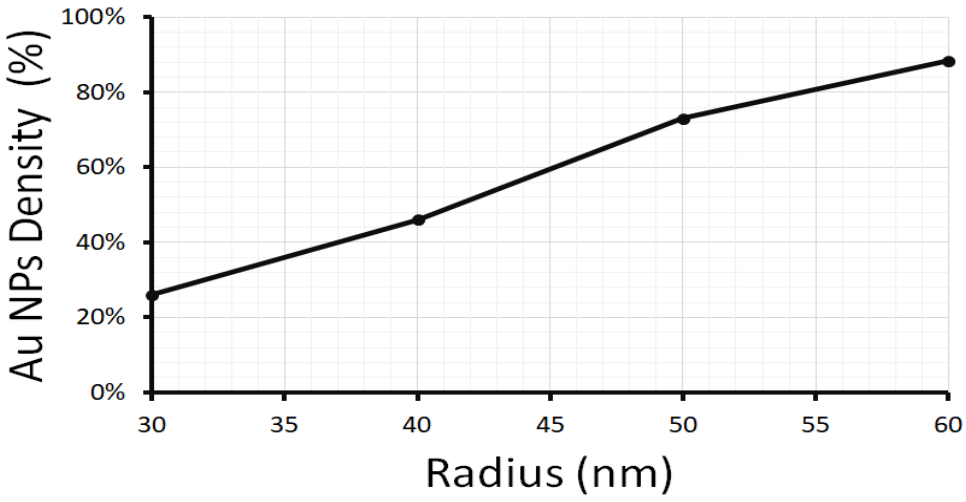

Figure 9. Au NP density for different radii: 30, 40, 50, and 60 nm.

To calculate the Au NP density, the area of all distributed NPs in the unit cell is divided by the available area on the silicon substrate, without NWs.

The period, *P*, between each NW has a significant effect on the solar cell performance. So, the effect of changing the period from 350 to 600 nm on the short-circuit current density and power conversion efficiency is simulated and summarized in Table 6.

Table 6. Short-circuit current density and overall efficiency for different distances between NWs.

Period (nm)	J_{sc} (mA/cm^2)	PCE (%)
350	33.0	15.0
400	27.8	12.7
450	35.9	16.4
500	40.6	18.5
550	41.7	19.0
600	33.8	15.4

The optimum performance is obtained at period $P = 550$ nm, which gives $J_{sc} = 41.7$ mA/cm^2 and $PCE = 19.0\%$. The values of short-circuit current density and PCE decrease as the NW separation distance increases, larger than 500 nm, as the concept of multireflection of the incident light is decreased.

Moreover, the height of the NWs also plays a very important role in solar cell performance. Hence, the effect of NW length on the short-circuit current density and PCE is calculated with a change in the NW length from 3 to 6 µm as given in Table 7. The best performance has been obtained at 5 µm length, as the increase in the length will increase the electron relaxation due to changing the NW bandgap.

Table 7. Short-circuit current density and overall efficiency for different NW lengths.

NW height (μm)	J_{sc} (mA/cm^2)	PCE (%)
3	30.5	13.9
3.5	32.5	14.9
4	33.4	15.2
4.5	37.6	17.1
5	41.7	19.0
5.5	40.2	18.3
6	39.0	17.8

5. Optical Power Distribution

Optical power distribution is monitored at different layers, between the silicon substrate and back oxide, layer 1; at the top of Si substrate, layer 2; in the middle of the SiNWs, layer 3; and at the top of NWs, layer 4. Figure 10 shows the locations of the four layers.

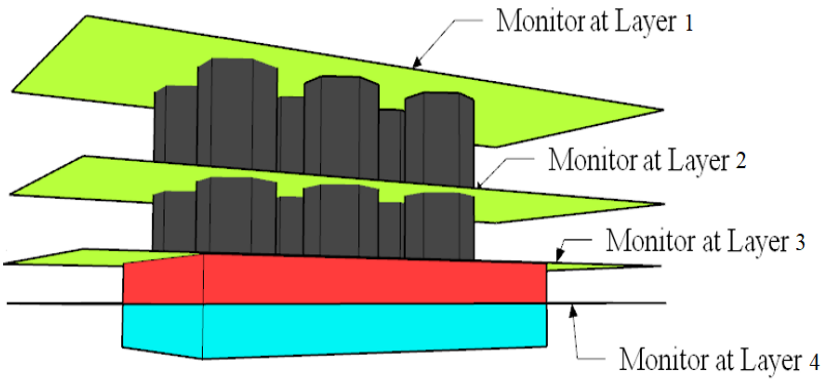

Figure 10. Different positions of electric field monitoring layers.

Figure 11 illustrates the optical power distribution on the four different monitoring layers for all proposed solar cells, traditional SiNWs, SiNWs with C layer, SiNWs with AuNPs, and SINWs with C and Au NPs.

Figure 11a, monitoring layer 1, shows the effect of the graphene layer on the top of NWs; it behaves like a nanoantenna, which retransmits the optical power into the active layer. Au NPs absorb the optical power on the substrate surface, as clearly shown in monitoring 2 with Au NPs; however, monitoring layers 3 and 4 have the same effect.

Finally, the proposed solar cell structure is compared to other structures in the literature, fabricated structures as in [1,5,6,13] and analytical analysis work as in [14], as illustrated in Table 8. The proposed structure does not give the maximum open-circuit voltage, 0.63 V, or *FF*, 0.73; however, it produces a high short-circuit current density, 41.7 mA/cm^2, and consequently a high value of the power conversion efficiency, 19.0%.

Table 8. Comparison between other solar cells and the proposed structure.

Different Structure	V_{oc} (V)	FF	J_{sc} (mA/cm^2)	PCE (%)
[5]	0.56	0.61	17.3	5.31
[6]	0.47	0.59	13.7	3.80
[1]	0.82	0.73	15.2	9.30
[13]	0.51	0.61	33.6	11.61
[14]	0.76	0.86	38.8	-
Proposed structure	0.63	0.73	41.7	19.00

In brief, the main advantage of this study is that the proposed structure enhances the absorption of the SiNWs in the NIR region in addition to the visible region, which leads to improvement in the overall solar cell performance.

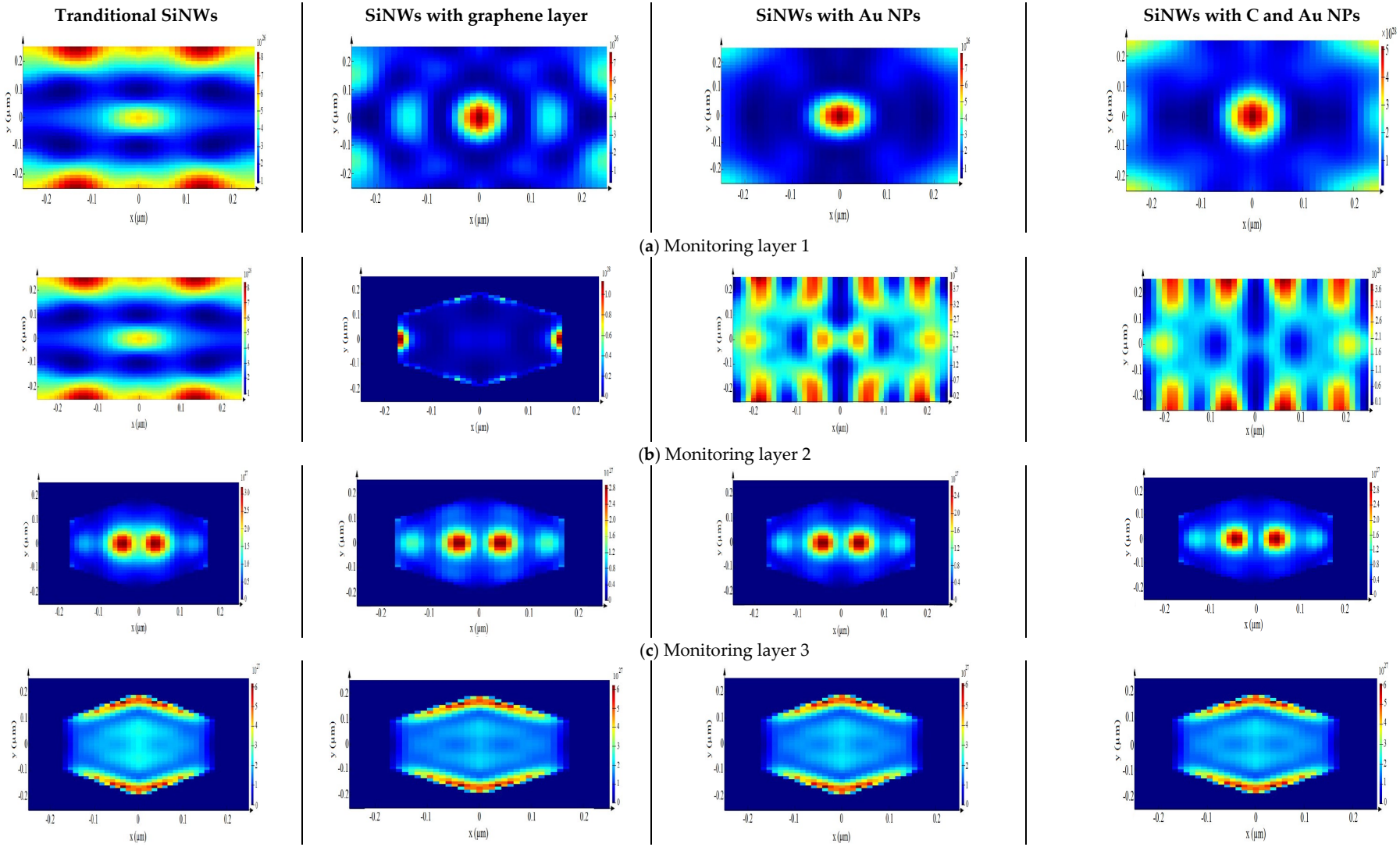

Figure 11. Optical power distribution at different monitoring layers for four different proposed structures.

6. Conclusions

In the proposed solar cell, the top surface of the SiNWs is coated with a graphene layer and the plasmonic Au NPs are distributed on the silicon surface. An FDTD method is used to calculate the optical power absorption and short-circuit current density of a SiNW solar cell. The open-circuit voltage, fill factor, and power conversion efficiency are calculated using numerical analysis. The maximum obtained optical power efficiency is 19.0% for J_{sc} = 41.7 mA/cm^2, V_{oc} = 0.63 V, and FF = 0.73. In addition, the optimum Au NP radius is 50 nm and the excess carrier concentration value is 1×10^{-15} cm^{-3}. The best performance of the introduced solar cell is obtained when Au NPs are used as a plasmonic material, rather than Ag, Al, or Cu materials. Moreover, the optimum NW length is simulated, L = 5 µm, and the distance between two NWs, P = 550 nm, is also calculated. In addition, optical power distribution inside the NWs, on the silicon substrate, and in the interface between substrate and oxide layer shows that the graphene layer and Au NPs behave as nanoantennas by retransmitting the trapped light from the surface into the active layer of the solar cell.

Funding: This research received no external funding.

Institutional Review Board Statement: Not applicable.

Informed Consent Statement: Not applicable.

Data Availability Statement: Not applicable.

Conflicts of Interest: There is no conflict of interest.

References

1. Yu, L.; Cabarrocas, P. Polymorphous nano-si and radial junction solar cells. In *Handbook of Photovoltaic Silicon*; Springer: Berlin/Heidelberg, Germany, 2018.
2. Street, R.; Qi, P.; Lujan, R.; Wong, W. Reflectivity of disordered silicon nanowires. *Appl. Phys. Lett.* **2008**, *93*, 163109. [CrossRef]
3. Street, R.; Wong, W.; Paulson, C. Analytic model for diffuse reflectivity of silicon nanowire mats. *Nano Lett.* **2009**, *9*, 3494–3497. [CrossRef] [PubMed]
4. Brönstrup, G.; Jahr, N.; Leiterer, C.; Csáki, A.; Fritzsche, W.; Christiansen, S. Optical properties of individual silicon nanowires for photonic devices. *ACS Nano* **2010**, *4*, 7113–7122. [CrossRef] [PubMed]
5. Garnett, E.; Yang, P. Light trapping in silicon nanowire solar cells. *Nano Lett.* **2010**, *10*, 1082–1087. [CrossRef]
6. Wallace, S.; Jevasuwan, W.; Fukata, N. Silicon nanowires covered with on-site fabricated nanowire-shape graphene for schottky junction solar cells. *Sol. Energy* **2021**, *224*, 666–671. [CrossRef]
7. Li, X.; Zhu, H.; Wang, K.; Cao, A.; Wei, J.; Li, C.; Jia, Y.; Li, Z.; Li, X.; Wu, D. Graphene-on-silicon Schottky junction solar cells. *Adv. Mater.* **2010**, *22*, 2743–2748. [CrossRef]
8. Liu, X.; Zhang, W.; Meng, H.; Yin, G.; Zhang, Q.; Wang, L.; Wu, L. High efficiency schottky junction solar cells by co-doping of graphene with gold nanoparticles and nitric acid. *Appl. Phys. Lett.* **2015**, *106*, 233901. [CrossRef]
9. Elrashidi, A. Electrophotonic improvement of polymer solar cells by using graphene and plasmonic nanoparticles. *Mater. Express* **2017**, *7*, 1–7. [CrossRef]
10. Huang, Y.; Liang, H.; Zhang, Y.; Yin, S.; Cai, C.; Liu, W.; Jia, T. Vertical tip-to-tip interconnection p–n silicon nanowires for plasmonic hot electron-enhanced broadband photodetectors. *ACS Appl. Nano Mater.* **2021**, *4*, 1567–1575. [CrossRef]
11. Jbira, E.; Derouiche, H.; Missaoui, K. Enhancing effect of silver nanoparticles (AgNPs) interfacial thin layer on silicon nanowires (SiNWs)/PEDOT: PSS hybrid solar cell. *Sol. Energy* **2020**, *211*, 1230–1238. [CrossRef]
12. Shin, D.; Kim, J.; Kim, H.J.; Jang, C.; Seo, S.; Lee, H.; Kim, S.; Choi, S. Graphene/porous silicon Schottky-junction solar cells. *J. Alloys Compd.* **2017**, *715*, 291–296. [CrossRef]
13. Yoon, J.; Baca, A.; Park, S.; Elvikis, P.; Geddes, J.; Li, L.; Kim, R.; Xiao, J.; Wang, S.; Kim, T.; et al. Ultrathin silicon solar microcells for semitransparent, mechanically flexible and microconcentrator module designs. *Nat. Mater.* **2008**, *7*, 907–915. [CrossRef] [PubMed]
14. Augusto, A.; Herasimenka, S.; King, R.; Bowden, S.; Honsberg, C. Analysis of the recombination mechanisms of a silicon solar cell with low bandgap-voltage offset. *J. Appl. Phys.* **2017**, *121*, 205704. [CrossRef]
15. Zhou, F.; Qin, F.; Yi, Z.; Yao, W.; Liu, Z.; Wu, X.; Wu, P. Ultra-wideband and wide-angle perfect solar energy absorber based on Ti nanorings surface plasmon resonance. *Phys. Chem. Chem. Phys.* **2021**, *23*, 17041–17048. [CrossRef]
16. Deng, Y.; Cao, G.; Wu, Y.; Zhou, X.; Liao, W. Theoretical Description of Dynamic Transmission Characteristics in MDM Waveguide Aperture-Side-Coupled with Ring Cavity. *Plasmonics* **2015**, *10*, 1537–1543. [CrossRef]

17. Deng, Y.; Cao, G.; Yang, H.; Zhou, X.; Wu, Y. Dynamic Control of Double Plasmon-Induced Transparencies in Aperture-Coupled Waveguide-Cavity System. *Plasmonics* **2018**, *13*, 345–352. [CrossRef]
18. Zheng, Z.; Zheng, Y.; Luo, Y.; Yi, Z.; Zhang, J.; Liu, Z.; Yang, W.; Yu, Y.; Wu, X.; Wu, P. A switchable terahertz device combining ultra-wideband absorption and ultra-wideband complete reflection. *Phys. Chem. Chem. Phys.* **2022**, *24*, 2527–2533. [CrossRef]
19. Zhao, F.; Lin, J.; Lei, Z.; Yi, Z.; Qin, F.; Zhang, J.; Liu, L.; Wu, X.; Yang, W.; Wu, P. Realization of 18.97% theoretical efficiency of 0.9 μm thick c-Si/ZnO heterojunction ultrathin-film solar cells via surface plasmon resonance enhancement. *Phys. Chem. Chem. Phys.* **2022**, *24*, 4871–4880. [CrossRef]
20. Yang, X.; Wang, D. Photocatalysis: From Fundamental Principles to Materials and Applications. *ACS Appl. Energy Mater.* **2018**, *1*, 6657–6693. [CrossRef]
21. Nan, T.; Zeng, H.; Liang, W.; Liu, S.; Wang, Z.; Huang, W.; Yang, W.; Chen, C.; Lin, Y. Growth Behavior and Photoluminescence Properties of ZnO Nanowires on Gold nano-particle Coated Si Surfaces. *J. Cryst. Growth* **2012**, *340*, 83–86. [CrossRef]
22. Kang, Z.; Gu, S.; Yan, Q.; Bai, M.; Liu, H.; Liu, S.; Zhang, H.; Zhang, Z.; Zhang, J.; Zhang, Y. Enhanced Photoelectrochemical Property of ZnO Nanorods Array Synthesized on Reduced Graphene Oxide for Self-powered Biosensing Application. *Biosens. Bioelectron.* **2015**, *64*, 499–504. [CrossRef] [PubMed]
23. Kang, Z.; Yan, Q.; Wang, F.; Bai, M.; Liu, C.; Zhang, Z.; Lin, P.; Zhang, H.; Yuan, G.; Zhang, J.; et al. Electronic Structure Engineering of Cu_2O Film/ZnO Nanorods Array All-oxide p-n Heterostructure for Enhanced Photoelectrochemical Property and Self-powered Biosensing Application. *Sci. Rep.* **2015**, *5*, 7882. [CrossRef] [PubMed]
24. Sinton, R.; Cuevas, A. Contactless determination of current–voltage characteristics and minority-carrier lifetimes in semiconductors from quasi-steady-state photoconductance data. *Appl. Phys. Lett.* **1996**, *69*, 2510. [CrossRef]
25. Aspnes, D.; Studna, A. Dielectric functions and optical parameters of Si, Ge, GaP, GaAs, GaSb, InP, InAs, and InSb from 1.5 to 6.0 eV. *Phys. Rev.* **1983**, *27*, 985. [CrossRef]
26. Phillip, H.; Taft, E. Kramers-Kronig Analysis of Reflectance Data for Diamond. *Phys. Rev.* **1964**, *136*, A1445. [CrossRef]
27. Elrashidi, A.; Tharwat, M. Broadband absorber using ultra-thin plasmonic metamaterials nanostructure in the visible and near-infrared regions. *Opt. Quantum Electron.* **2021**, *53*, 426. [CrossRef]